IEEE Journal of Microwaves

Received 4 June 2021; revised 7 July 2021; accepted 25 July 2021. Date of publication 31 August 2021; date of current version 7 October 2021.

Digital Object Identifier 10.1109/JMW.2021.3100765

System Performance of a Scalable 79 GHz Imaging MIMO Radar With Injection-Locked LO Feedthrough

DOMINIK SCHWARZ [1] (Graduate Student Member, IEEE), CHRISTIAN MEYER [1], ANDRÉ DÜRR [1] (Graduate Student Member, IEEE), AHMAD MUSHTAQ [2] (Member, IEEE), WOLFGANG WINKLER [2] (Member, IEEE), AND CHRISTIAN WALDSCHMIDT [1] (Senior Member, IEEE)

[1]Institute of Microwave Engineering, Ulm University, 89081 Ulm, Germany
[2]Silicon Radar GmbH, 15236 Frankfurt (Oder), Germany

CORRESPONDING AUTHOR: Dominik Schwarz (e-mail: dominik-1.schwarz@uni-ulm.de).

The development of the MMICs used in this work was supported by the German Federal Ministry of Education and Research within the KAMERAD-Project (BMBF FKZ 16ES0574).

ABSTRACT The estimation of the direction-of-arrival in a coherent multi-channel radar system requires the distribution of the high-frequency local oscillator signal to all hardware channels. Various system concepts with distribution network or feedthrough topologies are established. While distribution networks are bulky and costly, the time delays in systems with a feedthrough topology cause systematic errors in the range evaluation. In this work, a system concept based on an injection-locked feedthrough and the related radar system analysis is presented. The disadvantage of time delays in common feedthrough architectures can be eliminated by a hardware correction using the phase shifting capabilities of the injection-locked oscillator. In addition, two software correction algorithms are presented and analyzed. The performance of the realized system is shown by radar measurements and direction-of-arrival estimations. It is proven that the phase noise of different injection-locked oscillators is fully correlated within the radar system which results in the same detection performance as in state-of-the-art radar systems using a signal distribution network. Thus, the injection-locked feedthrough imaging radar topology is a suitable concept of realizing flexible radar frontends without bulky distribution networks.

INDEX TERMS Automotive radar, chirp sequence modulation, coherency, direction-of-arrival (DoA) estimation, frequency modulated continuous wave (FMCW), injection-locking, imaging radar, local oscillator (LO) feedthrough, mm-wave, monolithic microwave integrated circuit (MMIC), multiple-input multiple-output (MIMO), phase noise correlation, time delay correction.

I. INTRODUCTION

Imaging radar sensors are used in a wide range of applications as they provide accurate information of range, velocity, and direction-of-arrival (DoA) of the targets [1]–[4]. The radars in advanced driver assistance systems (ADAS) and other automotive applications operate in the 77/79 GHz frequency band and employ the multiple-input multiple-output (MIMO) principle [5]–[7]. In order to be able to perform DoA estimations, phase coherence and therefore a constant phase relationship between the hardware channels must be ensured. Especially for radar systems with a high channel count, the signal distribution requires a lot of space and is associated with a high effort in terms of design time and hardware cost. Imbalances due to different time delays or phase variations of the components lead to systematic errors in the radar measurement. Simultaneously, the cost, reliability, and size restrictions for mass-produced automotive systems have to be adhered [6]. Therefore, the signal distribution concept is an important aspect of the system design. An overview and comparison of state-of-the-art radar systems is given in Table 1.

To ensure both coherency and correlated phase noise, most radar systems share a centrally generated frequency modulated continuous wave (FMCW) signal. Typically, the signal is distributed in a star or tree topology

TABLE 1. Overview of mm-Wave Imaging Radar Systems

Source	f / GHz	N_{Vx}	B / GHz	System Concept
[8]	77	8 or 16	2	Distribution
[9]	79	4	9	Distribution
[10]	120	576	5	Distribution
[11]	79	192	5	Distribution
[12]	77	128	2	Distribution
[13]	79	4	8	Feedthrough
[14]	120	16	5	Feedthrough
This work	79	64	10	ILO feedthrough

using power splitters. For a signal distribution at the operating frequency [8], the high losses on a printed circuit board (PCB) limit the maximum transmission line length and therefore the size of the radar sensor. To overcome this limitation, the FMCW signal is often distributed at a lower frequency and is later multiplied or up-converted within the radar monolithic microwave integrated circuit (MMIC) [9]. This also enables operating frequencies above 100 GHz [10]. Due to the losses of the distribution networks, the FMCW signal has to be generated with a high output power or to be amplified within the distribution network [11], [12].

With an increasing channel count, the distribution networks are more and more complex, especially if the signal line lengths are matched. This results in a large space requirement on the PCB and additionally needed amplifiers (integrated or assembled on the PCB) and therefore increased costs. By feeding the FMCW signal through all MMICs in a daisy-chained manner [13], [14], these drawbacks can be overcome. Since the FMCW signal is generated by a single local oscillator (LO), such systems are denoted as LO feedthrough [15]. This comes at the cost of different time delays of the FMCW signal in the hardware channels, which result in systematic measurement errors.

In this contribution, a system concept based on an injection-locked LO feedthrough topology is presented. Like in conventional systems with LO feedthrough, no bulky FMCW signal distribution network is needed. The injection-locked oscillator (ILO) in each MMIC locks even for a weak input power [16]. Therefore and almost regardless of the LO input power, a more robust system operation as in conventional LO feedthrough systems and a constant transmit power is facilitated. A phase noise analysis [17], [18] of the realized injection-locked radar system is provided and proven by radar measurements. This extends the general theory of concatenated ILOs reported in [19]–[21]. By means of the phase shifting capabilities of an ILO [22], the systematic errors caused by the time delays in the daisy-chained signal distribution can be corrected. This hardware correction is compared to a software correction.

This paper is organized as follows: The system concept is introduced in Section II. In Section III, a system analysis of the influence of the phase noise on the detection performance and the effect and correction of the signal delay between the hardware channels is given. The derived conclusions are verified by radar measurements in Section IV.

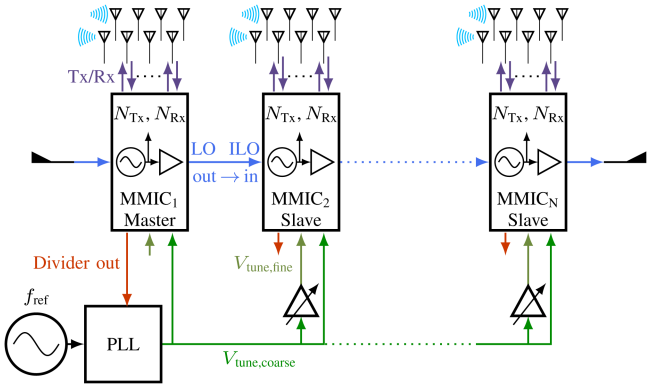

FIGURE 1. Block diagram of the scalable imaging radar system with injection-locked LO feedthrough topology. The system is composed of N MMICs, each one incorporating N_{Tx} Tx and N_{Rx} Rx channels.

II. SYSTEM CONCEPT

The proposed system, as sketched in Fig. 1, is composed of N MMICs, each incorporating multiple transmit (Tx) and receive (Rx) channels. Compared to MMICs used for conventional LO feedthrough the LO input amplifier is replaced by an ILO [16]. This eliminates the need for an external voltage controlled oscillator (VCO) and thus reduces both power consumption and component count. The LO outputs are directly connected to the following ILO inputs in a daisy-chained manner. The FMCW signal is generated in the master MMIC with an external phase-locked loop (PLL) in the ILO frequency range and later multiplied within the MMICs. All other ILOs in the slave MMIC are loosely aligned to the FMCW signal by the coarse tuning voltage that is applied to all MMICs. This ensures that the free-running frequency of the individual ILOs is close to the instantaneous frequency of the FMCW signal. As all slaves lock on their ILO input signal, which is generated by the master or the antecedent slave, phase coherency is achieved [22]. Thus, the criterion of frequency and phase synchronization [23] is fulfilled, and DoA estimations are enabled. Additionally, a fine adjustment of the free-running frequency is possible with the fine tuning voltage. This enables the operation of the slave ILOs in the locked state as phase shifters.

III. SYSTEM ANALYSIS

In the beginning of this section, the phase noise (PN) of the injection-locked radar system is analyzed regarding the correlation of the PN from different locked ILOs. Afterwards, the effect and the correction of a time delay between the radar MMICs is investigated.

A. PHASE NOISE OF THE ILO RADAR SYSTEM

In case of strong targets, the noise level in the intermediate frequency (IF) spectrum is increased by the PN of the FMCW

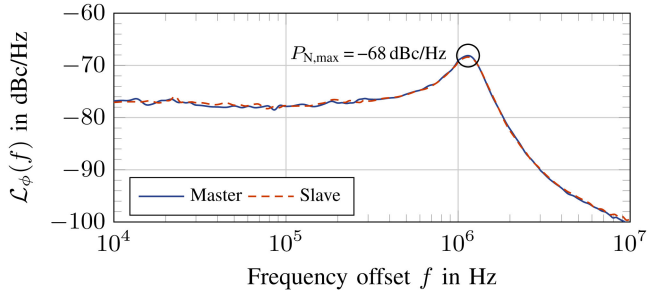

FIGURE 2. Measured PN at the radar center frequency $f_c = 78.5$ GHz.

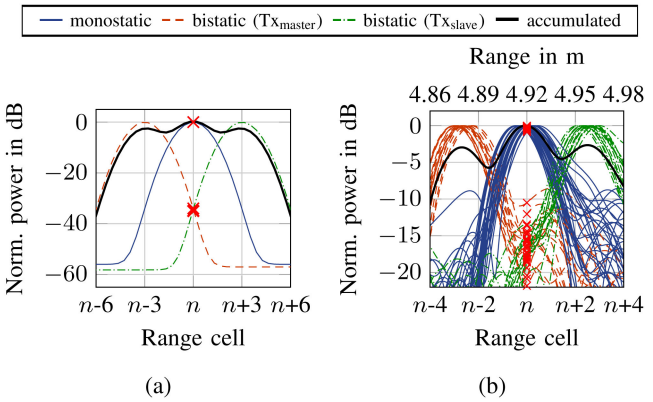

FIGURE 3. Range spectra for two in a daisy-chain synchronized MMICs and a single target located at range cell *n:* (a) simulated range spectra for single channel MMICs with a shift of the bistatic results by three range cells; (b) measured range spectra with 64 radar channels, a bandwidth of 10 GHz, and a delay Δt_0 corresponding to a shift of 2.7 range cells.

signal. This reduces the detection performance for weak targets that are located close to strong ones [18].

For the proposed radar system, MMICs of the same type are used as master and slave. Thus, the phase noise power density curves are identical, which is verified by measurements at the center frequency of the FMCW signal, see Fig. 2. The phase noise curves remain unchanged by the injection-locking, since they are already identical [20].

As the signal phase of the slave ILO is locked to that of the master ILO [22], the phase noise is correlated within the locking range. The locking range of the used MMIC is larger than 300 MHz [16]. This clearly exceeds the IF frequency range of 50 MHz which allows the assumption of a full PN correlation. In this case, the residual phase noise at the output of the mixer $\mathcal{L}_{\Delta\Phi}(f)$ is reduced due to the range correlation effect [24] and is given by

$$\mathcal{L}_{\Delta\Phi}(f) = \mathcal{L}_{\Phi}(f) \cdot 2\Big(1 - \cos\left(2\pi f \tau\right)\Big), \tag{1}$$

where $\mathcal{L}_{\Phi}(f)$ denotes the PN density in the FMCW signal, f the frequency offset from the carrier, and τ the signal delay in the radar channel. Since this effect applies like in radar systems with a distribution network, a high phase noise reduction for targets at small distances is expected. This results in a prevalence of the thermal noise influence [17].

B. LO INPUT DYNAMIC RANGE

The maximum input power of the ILO is limited by the maximum power level of the LO output amplifier, which is at least −2 dBm for the used MMIC [16], and the loss of the MMIC-to-MMIC transition, which can be approximated with 2 dB. For the minimum ILO input power of −22 dBm the locking range is reduced but is still larger than 85 MHz, which fully covers typical IF frequency ranges. At lower input power levels the ILO loses the locked state and the frequency and phase coherence vanish, making the radar system inoperable. This leads to a wide dynamic range of the ILO input port of 18 dB (−22 dBm ... −4 dBm) proving the high tolerance to different input power levels. In contrast, the LO input dynamic range of typical state-of-the-art MMICs as used in [11] is only half over the full operating temperature range (−6 dBm ... 3 dBm).

C. DELAY BETWEEN MMICS

If the signal is transmitted by one MMIC and received by another one (bistatic case), an additional time delay Δt_0 w.r.t. to the channel delay may occur:

$$\Delta t_0 = t_{0,\,\mathrm{Rx}} - t_{0,\,\mathrm{Tx}}\,. \tag{2}$$

This is the delay of the fed through FMCW signal, where t_0 is the ramp start time at the individual MMICs. Using the FMCW equation [25]

$$f_\mathrm{b} = \frac{B}{T}\tau \quad \text{with} \quad \tau = \frac{2R}{c_0}\,, \tag{3}$$

where f_b denotes the beat frequency, B the radar bandwidth, T the ramp duration, R the range, and c_0 the speed of light, the time delay is translated to a shift of the beat frequency

$$f_\mathrm{b} = \frac{B}{T}\left(\tau - \Delta t_0\right)\,. \tag{4}$$

For a positive delay, this results in a reduced beat frequency, and the radar target appears closer. This effect applies to all radar systems but can easily be omitted if signal distribution networks with equal signal line lengths are used.

The effect is shown by a simulation as illustrated in Fig. 3(a). In the case of two MMICs, half of the bistatic radar responses appear closer, whereas the other half appear further apart. This leads to a broadened peak in the accumulated signal, decreasing the target separability.

Typically, the phase values are extracted from the single range cell where the accumulated target peak is detected [26]. Due to the shift of the range spectra, the bistatic channels have a lower signal-to-noise ratio (SNR). This is indicated in Fig. 3 with red crosses and results in an inferior DoA estimation performance. In Fig. 3(b) this effect is shown for measurements with a delay Δt_0 corresponding to a shift of 2.7 range cells and leading to an SNR reduction of up to 20 dB.

The constant beat frequency offset can also be expressed as a linearly rising phase difference between the FMCW signals

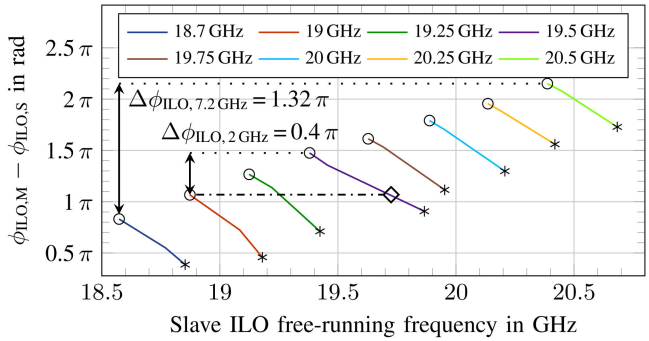

FIGURE 4. Measured phase difference between master ILO and injection-locked slave ILO versus the slave ILO free-running frequency with disabled injection locking. Different CW frequencies of the master ILO are plotted between minimum (○) and maximum slave fine tuning voltage (∗).

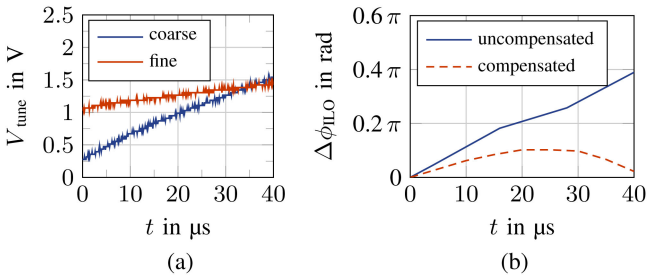

FIGURE 5. Phase compensation for an FMCW ramp with a bandwidth of 2 GHz: (a) tuning voltages applied to slave in compensated case and (b) relative phase difference between master and slave ILO.

of the master and slave MMICs. The phase difference $\Delta\phi$ at the end of the FMCW ramp is [16]

$$\Delta\phi = 2\pi B \Delta t_0 \,. \tag{5}$$

Often, the ILO signal is distributed in a lower frequency range, and a frequency multiplication is performed within the MMICs. Thus, the multiplication factor M_{ILO} has to be taken into account to calculate the phase difference in the ILO frequency range:

$$\Delta\phi_{\mathrm{ILO}} = 2\pi \frac{B}{M_{\mathrm{ILO}}} \Delta t_0 \,. \tag{6}$$

HARDWARE CORRECTION

This phase difference can be compensated by means of the ILOs phase shifting capabilities as stated in Section II. The maximum compensable time delay is

$$\Delta t_{0,\mathrm{max}} = \frac{1}{4}\frac{M_{\mathrm{ILO}}}{B} \,, \tag{7}$$

as the maximum achievable phase shift with a locked ILO is $\Delta\phi_{\mathrm{ILO,max}} = \pi/2$ rad [22]. Using the range resolution $\delta R = c_0/(2B)$ [5] and the delay of a transmission line on a PCB [27]

$$t = L\frac{\sqrt{\varepsilon_{\mathrm{r,eff}}}}{c_0} \,, \tag{8}$$

with the line length L and the effective relative permittivity $\varepsilon_{\mathrm{r,eff}}$ for the transmission line, (7) can be rewritten as

$$\Delta L_{\mathrm{max}} = \frac{M_{\mathrm{ILO}}}{2\sqrt{\varepsilon_{\mathrm{r,eff}}}} \delta R \,. \tag{9}$$

This gives an upper limit for transmission line lengths, for which a hardware correction of the beat frequency offset is possible. With (3), (8), and (9), the corresponding range offset ΔR in relation to the range resolution is given by

$$R = L\frac{\sqrt{\varepsilon_{\mathrm{r,eff}}}}{2} \quad \rightarrow \quad \Delta R_{\mathrm{max}} = \frac{M_{\mathrm{ILO}}}{4}\delta R \,. \tag{10}$$

The range offset is only half of the transmission line length due to the two-way propagation of the radar signal. Regardless of the bandwidth, the maximum range cell offset to be compensated and thus the amount of SNR reduction remain constant. For larger bandwidths both shorter absolute transmission line length differences can be compensated and the severity of the SNR reduction increases. These limitations can be diminished by increasing M_{ILO} and therefore distributing the ILO signal at a lower frequency.

In Fig. 4, the phase difference between master and slave MMIC is shown for the proposed system and $M_{\mathrm{ILO}} = 4$ [16]. For a constant fine tuning voltage at the slave, e.g. the minimum value (○), the phase difference rises with the ILO frequency. For a radar bandwidth of 7.2 GHz, the phase difference $\Delta\phi_{\mathrm{ILO,\,7.2\,GHz}}$ is 1.32 π rad, which can not be compensated as it is larger as $\pi/2$ rad. In the following, the hardware correction is investigated for a radar bandwidth of 2 GHz and a ramp start frequency of 76 GHz. This corresponds to an ILO frequency range from 19 GHz to 19.5 GHz. In this case, the phase difference $\Delta\phi_{\mathrm{ILO,\,2\,GHz}}$ is 0.4 π rad which corresponds to an effective transmission line length between both MMICs of 75 mm.

Applying the fine tuning voltage to the slave MMIC with disabled injection locking, the free-running frequency changes. This is shown by the abscissas in Fig. 4. However, in the locked state, the slave ILO operates as phase shifter, and the instantaneous frequency of master and slave remains identical [22]. To compensate for the transmission line length, the phase difference $\Delta\phi_{\mathrm{ILO}}$ must remain constant, which is indicated in Fig. 4 with a dash-dotted line.

The tuning voltages for the FMCW ramp with a duration of 40 μs are shown in Fig. 5(a). Due to non-idealities in the proposed system, the phase difference $\Delta\phi_{\mathrm{ILO}}$ shown in Fig. 5(b) can not be compensated perfectly. To analyze the remaining error, the ILO phase-slope $m_{\Delta\phi,\,\mathrm{ILO}}$ over the full ramp duration T,

$$m_{\Delta\phi,\,\mathrm{ILO}} = \frac{\Delta\phi_{\mathrm{ILO}}}{T} \,, \tag{11}$$

(4), and (6) are used to determine the beat frequency offset

$$\Delta f_{\mathrm{b}} = m_{\Delta\phi,\,\mathrm{ILO}} \frac{M_{\mathrm{ILO}}}{2\pi} \,. \tag{12}$$

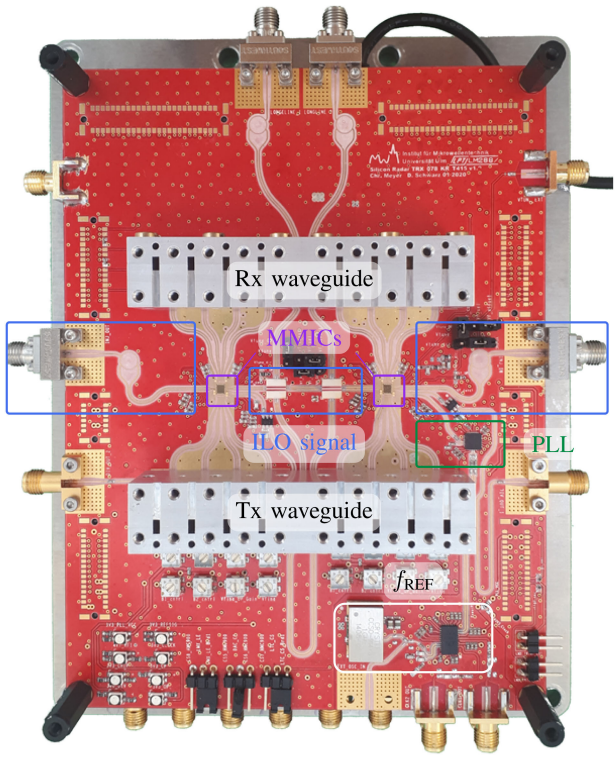

FIGURE 6. Photograph of the scalable radar demonstrator frontend.

The compensated phase difference (- - -) in Fig. 5(b) is zero at the end of the ramp and results in a vanished beat frequency offset and therefore a successful compensation. In the continuous time $t \in [0, T]$ the remaining slope of the compensated phase difference corresponds to ramp linearity errors and leads to a broadening of the target response in the frequency domain and thus to a reduced target separability. To correct this error, the fine tuning voltage can be generated with a digital-to-analog converter for the full compensation of the phase offset in the continuous time.

SOFTWARE CORRECTION

As the hardware correction cannot compensate offsets of more than a single range cell for the considered hardware setup, a software correction is derived in the following. This correction can also be applied to other radar systems with mismatched time delays. The range offset $\Delta R/\delta R$ is determined by a calibration measurement of a static target. This offset can be corrected in time-domain with the same algorithm as used for the correction of the range-angle coupling [26]:

$$s_{\mathrm{B,\,corr},\,k} = s_{\mathrm{B},\,k}(t)\exp\left(-2\pi \mathrm{j}\frac{\Delta R_k}{\delta R}\frac{t}{T}\right), \qquad (13)$$

with the corrected time-domain signal $s_{\mathrm{B,\,corr},\,k}$ of the virtual channel k, the raw time-domain signal $s_{\mathrm{B},\,k}(t)$, the continuous time $t \in [0, T]$, and the ramp duration T. This correction is computationally extensive, as a complex multiplication has to be performed per ramp, receive channel, and sample. On the other hand, it is possible to compensate offsets of less than a single range cell as with the hardware correction.

To reduce the computational effort, the range spectra obtained after the range-Doppler processing can be shifted in multiples of range bins [26]:

$$n_{\mathrm{shift},\,k} = \left\lfloor \frac{\Delta R_k}{\delta R} N_{\mathrm{ZP}} + 0.5 \right\rfloor . \qquad (14)$$

N_{ZP} denotes the applied zeropadding factor. A phase correction is not necessary, if this correction is identically applied both to calibration and measurement. As only offsets of entire range bins are corrected, the remaining range offset of up to 0.5 range bins leads to an SNR reduction of up to 4 dB, depending on the applied window function and N_{ZP}.

COMPARISON

The application of the hardware correction enables the correction of range shifts of up to one range cell in case of a frequency multiplication factor M_{ILO} of 4. By correcting this error in hardware it can be neglected in the signal processing chain, which makes the sensor applicable in various system configurations. Larger shifts result in a significant SNR deterioration and can only be corrected using a lower ILO frequency or with the proposed software correction algorithms. The software correction can be used for all FMCW radar systems.

IV. VERIFICATION BY RADAR MEASUREMENTS

The radar frontend is shown in Fig. 6. It consists of $N = 2$ MMICs, each equipped with $N_{\mathrm{Tx}} = 4$ Tx and $N_{\mathrm{Rx}} = 4$ Rx channels, and thus resulting in $N_{\mathrm{Vx}} = 64$ virtual channels. A block diagram of the used MMIC can be found in [16]. The ILO input of the master MMIC and the output of the slave are routed to SMA connectors. This enables the combination of multiple frontends to larger arrays. In addition to the ILO signals, both tuning voltages and trigger signals are distributed to all boards. The PLL reference is derived from a 1 GHz oscillator and fed to a clock distribution chip. Different antenna frontends can be used, since the radar signals are guided through waveguide transitions and Tx and Rx waveguide blocks. The antenna layout is shown in Fig. 7(a) together with the corresponding physical and virtual antenna positions (b). An overview of the radar parameters is given in Table 2.

TABLE 2. Overview of the Radar Parameters

Ramp duration T	40 µs
Ramp repetition time T_{r}	50 µs
Ramp start frequency f_0	74.8 GHz / 76 GHz*
RF bandwidth B	10 GHz / 2 GHz*
Number of chirps N_{c}	128 N_{Tx}
Number of virtual channels N_{Vx}	$64 = 8 \times 8$
Multiplexing scheme	TDM
Virtual aperture A_{V}	37.5 λ_0

*With applied hardware correction.

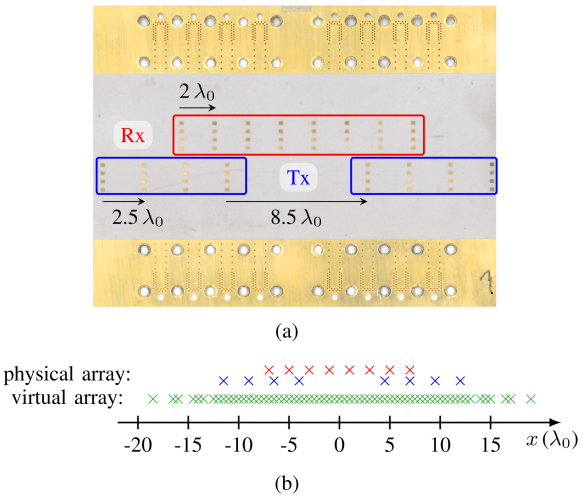

FIGURE 7. Antenna frontend of the radar demonstrator: (a) photograph and (b) sketch of the physical and virtual antenna array.

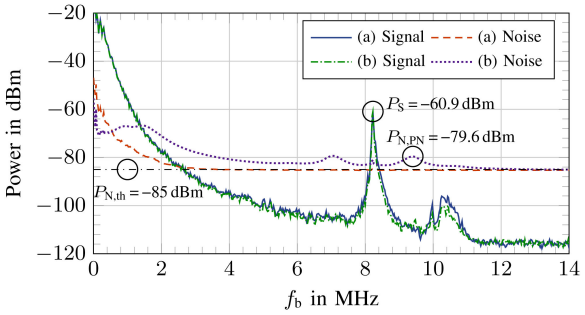

FIGURE 8. Range spectra for radar measurements with a bandwidth of 10 GHz of a very strong target (RCS = 28 m²) at a distance of 5 m: (a) with standard reference oscillator and (b) with worsened reference oscillator.

A. DETECTION PERFORMANCE

The phase noise correlation is proven by radar measurements. Therefore, the standard deviation of all FMCW ramps within a ramp block is used as indicator of the present noise in the measured data.

For a target at a distance of 5 m the maximum of the PN density in the range spectrum is −80 dBc/Hz. It is calculated using (1) for a PN in the FMCW signal of −68 dBc/Hz at a frequency offset of 1.15 MHz (see Fig. 2). Due to the evaluation with a Fourier transform (FT), the noise density is integrated over the width of a single range bin [28], leading to a peak of the PN at −36 dBc. For the radar measurement depicted in Fig. 8(a), this peak is at −97 dBm and below the thermal noise floor (−85 dBm) and therefore not visible.

To prove the PN model in Section III.A, the PN is artificially deteriorated by means of a significantly worsened reference oscillator, which increases the maximum PN by 18 dB. In this case, the PN is visible in the noise floor around the target, as can be seen in Fig. 8(b). Both location and level of the noise peak (−18.7 dBc at a frequency offset of 1.15 MHz) are consistent with the theory, demonstrating the full range correlation for injection-locked radar systems.

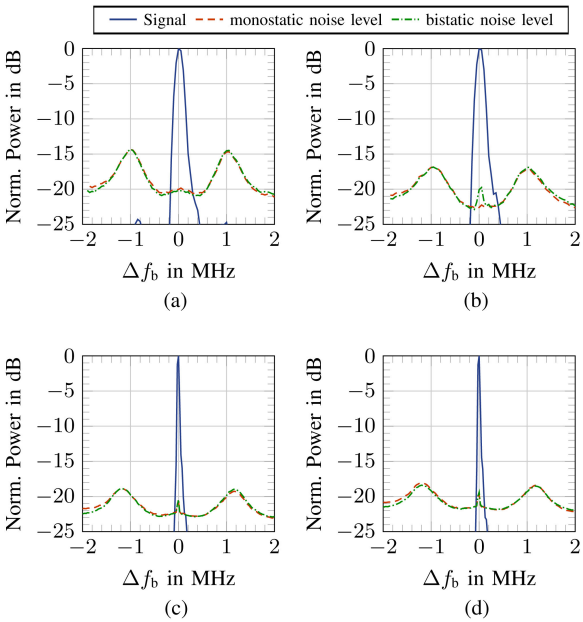

FIGURE 9. Relative PN with respect to the target response for radar measurements with worsened reference oscillator: (a) with a bandwidth of 2 GHz and no correction, (b) with a bandwidth of 2 GHz and applied hardware correction, (c) with a bandwidth of 10 GHz and software correction by multiples of range bins, and (d) as (c) but with a by 18 dB reduced injection input power at the slave.

For a more detailed analysis, the noise level is calculated for the mono- and bistatic channels for different system settings separately: reduced bandwidth with or without hardware correction, full bandwidth with software correction, and full bandwidth with correction and a reduced input power at the slave. The results are shown in Fig. 9(a)–(d). The noise level is identical in all cases for the mono- and bistatic channels. As the monostatic channels have an inherent PN correlation, this fully proves the correlation of the bistatic PN for the injection-locked radar systems in all use cases.

The deviations of the maximum PN value are due to the changes of the PLL and ILO behavior with the system settings for different bandwidths and correction methods. Thus, the PN profile of the FMCW signal changes. Additionally, the measurements depicted in Fig. 9(a) and (b) are measured with a reduced ramp time and therefore an increased noise bandwidth [28].

B. CORRECTION OF THE DELAY BETWEEN THE MMICS

In order to evaluate the performance and to compare the proposed correction methods introduced in Section III-C, FMCW radar measurements are performed. The measurements are evaluated with a combined frequency and phase evaluation using a discrete Fourier transform (DFT) [29], [30].

The results of 10 exemplary measurements with a radar bandwidth of 2 GHz are shown in Figs. 10(a) and (b) to indicate the functionality of the hardware correction. Without applying any correction (see Fig. 10(a)), different range results can be identified: about 5.07 m for Rx_1 to Rx_4, which

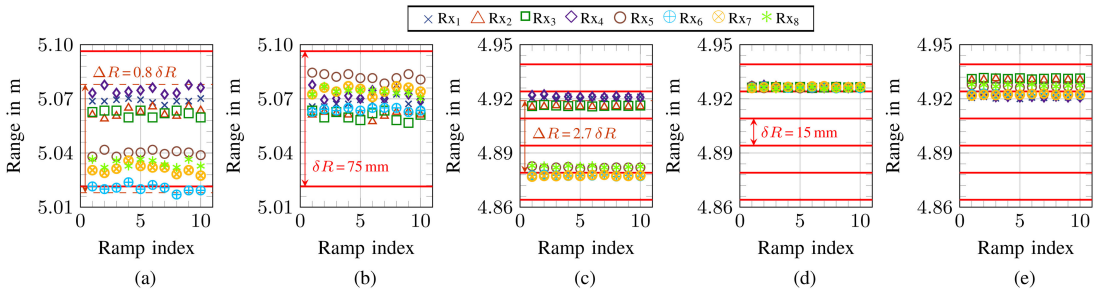

FIGURE 10. Evaluated range for 10 exemplary FMCW radar measurements with a Tx at the master, $Rx_{1\text{-}4}$ at the master, and $Rx_{5\text{-}8}$ at the slave MMIC. Corner reflector in a distance of 5.07 m, measured with a bandwidth of 2 GHz: (a) without correction and (b) with applied hardware correction. Corner reflector in a distance of 4.92 m, measured with a bandwidth of 10 GHz: (c) without correction, (d) with software correction in time domain, and (e) with software correction in multiples of range bins. The range cells are highlighted with red lines.

represent the monostatic case and are not affected by the delay between the MMICs and 5.03 m for Rx_5 to Rx_8 representing the bistatic case. As shown in (4), the target appears closer in those channels. The maximum range variation ΔR matches with the theory given by (10) and is 0.8 δR for an effective transmission line length of 75 mm. With applied hardware correction, the range offset of the bistatic channels is eliminated, and the targets are estimated at a similar range for all Rx channels, see Fig. 10(b). Additional deviations in the range occur due to antenna feed lines that are not length matched, as only errors induced by the delay between both MMICs can be compensated.

In Figs. 10(c)–(e) measurements with a radar bandwidth of 10 GHz are shown to analyze the performance of the software correction. For the bistatic case, the average range offset between the mono- and bistatic case is 2.7 δR, see Fig. 10(c). Using the time-domain software correction algorithm, all deviations can be corrected successfully with a precision of less than a single range cell, see Fig. 10(d).

The software correction in multiples of range bins is performed without zeropadding. In Fig. 10(e) it can be seen that the evaluated ranges for Rx_2 and Rx_3 are corrected by a single range cell and for Rx_5 – Rx_8 by three range cells. All evaluated ranges are within the width of a single range cell after the correction, which compensates for the most of the SNR reduction.

The higher standard deviation of the range measurements in Figs. 10(a) and (b) compared to (c) – (e) stems from the lower bandwidth, as the standard deviation of the range evaluation is inversely proportional to the bandwidth [31].

C. DOA ESTIMATION PERFORMANCE

To enable DoA estimation, the relative phases between the virtual channels must not change between different measurements for a target located at a fixed angle. First, the phase coherence is proven for the system with the ILO operating as phase shifter. The relative phases are exemplarily shown in Fig. 11. It can be seen that the relative phase of the individual virtual channels remains constant regardless of whether power cycles are performed between the measurements or whether the measurements are taken continuously. For the software correction identical mathematical operations are performed

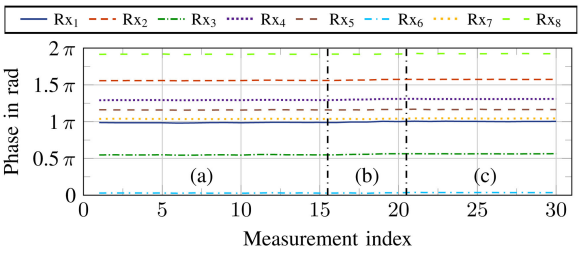

FIGURE 11. Evaluated relative phase of the radar response for a fixed target in 30 exemplary FMCW radar measurements with applied hardware correction and a Tx at the master, $Rx_{1\text{-}4}$ at the master, and $Rx_{5\text{-}8}$ at the slave MMIC: (a) with power cycles between the measurements, (b) continuous measurements without power cycles, and (c) with power cycles after a short pause.

TABLE 3. SNR Recovery and Phase Estimation Performance

	Monostatic channels		Bistatic channels	
Correction algorithm	SNR in dB	$\sigma_{\phi,\text{eval}}$ in rad	SNR in dB	$\sigma_{\phi,\text{eval}}$ in rad
None	27.2	$0.0140\,\pi$	8.8	$0.1927\,\pi$
Bin-shift	27.2	$0.0139\,\pi$	27.8	$0.0131\,\pi$
Time-domain	27.3	$0.0133\,\pi$	28.0	$0.0128\,\pi$

for each measurement. Therefore, an existing phase coherence of the underlying radar system is retained.

The correction capabilities for larger length mismatches are shown in Table 3 for radar measurements with a bandwidth of 10 GHz and different correction algorithms. The average SNR and the standard deviation of the complex 2D-FT result is calculated for a fixed target in 1280 exemplary FMCW radar measurements. No SNR reduction is present for monostatic channel combinations. As the standard deviation of the evaluated phases is small, no degradation in the DoA estimation performance has to be expected. For the bistatic channels, the shift of 2.7 range cells (see Fig. 10(c)) leads to an SNR reduction of almost 20 dB (see also Fig. 3(b)). According to theory, the correction in time-domain can fully recover the SNR in the bistatic channel combinations, restoring a low standard deviation of the evaluated phase as in the monostatic channels. With the software correction in multiples of the bin size almost the full SNR can be recovered, which makes it a suitable alternative.

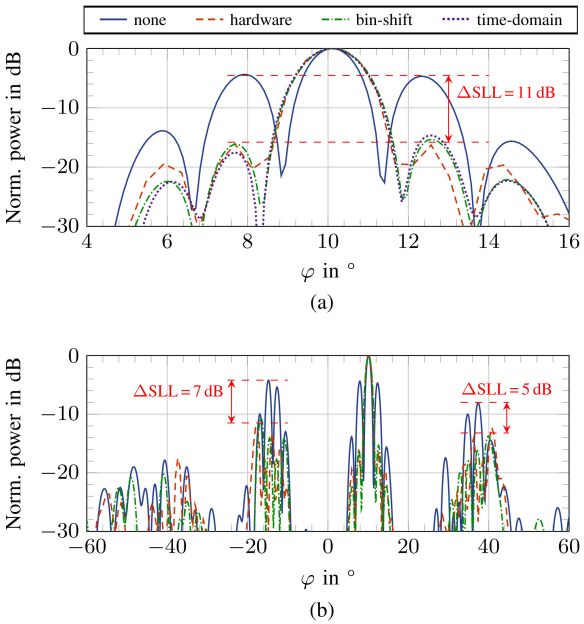

FIGURE 12. Angle estimation of a target in a distance of 5 m at an azimuth angle of approximately $\varphi = 10°$ for different length compensation methods: (a) mainlobe and (b) full angular pattern.

The DoA estimation performance is shown in Fig. 12. Performing radar measurements with a bandwidth of 10 GHz and without any correction leads to a by 11 dB increased sidelobe level (SLL), see Fig. 12(a). This is due to the SNR reduction in the bistatic channels, as these channels do not contribute significant information to the angle estimation. The SNR recovery of all correction methods is sufficient to recover the undistorted SLL of 16 dB. Regardless of the correction method, also the higher sidelobes at $\pm 25°$ distance to the mainlobe are reduced by 5 dB or 7 dB, restoring the overall SLL of more than 12 dB, see Fig. 12(b).

V. CONCLUSION

In this paper, a novel system for an imaging radar based on an injection-locked LO feedthrough topology and the related system analysis is presented. The proposed system is compact like systems with a feedthrough topology and is additionally also highly tolerant to different input power levels of the ILO. It is shown that the phase noise of different ILOs is fully correlated and the range correlation effect occurs. Therefore, the same detection performance as in radar systems with a signal distribution network is achieved without the need for the bulky and costly distribution network. The drawbacks in feedthrough topologies due to unmatched time delays are eliminated by the proposed hardware correction using the phase shifting capabilities of the ILO. Deviations of up to a whole range cell can be compensated with the given setup. This capability can be further increased if the ILO signal is distributed at a lower frequency range and multiplied within the MMICs. Larger length differences can be compensated using a software correction, which can be applied to all radar systems under the influence of mismatched time delays. The DoA estimations show that the ideal SLL of the antenna array is achieved, proving the phase coherency of the injection-locked radar system concept. In summary, the injection-locked feedthrough imaging radar topology is a promising concept of realizing flexible radar frontends.

REFERENCES

[1] P. Hügler, F. Roos, M. Schartel, M. Geiger, and C. Waldschmidt, "Radar taking off: New capabilities for UAVs," *IEEE Microw. Mag.*, vol. 19, no. 7, pp. 43–53, Nov. 2018.

[2] M. Zink *et al.*, "TanDEM-X: The new global DEM takes shape," *IEEE Geosci. Remote Sens. Mag.*, vol. 2, no. 2, pp. 8–23, Jun. 2014.

[3] S. S. Ahmed, A. Genghammer, A. Schiessl, and L.-P. Schmidt, "Fully electronic E-band personnel imager of 2 m^2 aperture based on a multistatic architecture," *IEEE Trans. Microw. Theory Techn.*, vol. 61, no. 1, pp. 651–657, Jan. 2013.

[4] W. Menzel, "Millimeter-wave radar for civil applications," in *Proc. 7th Eur. Radar Conf.*, 2010, pp. 89–92.

[5] J. Hasch, E. Topak, R. Schnabel, T. Zwick, R. Weigel, and C. Waldschmidt, "Millimeter-wave technology for automotive radar sensors in the 77 GHz frequency band," *IEEE Trans. Microw. Theory Techn.*, vol. 60, no. 3, pp. 845–860, Mar. 2012.

[6] J. Hasch, "Driving towards 2020: Automotive radar technology trends," in *Proc. IEEE MTT-S Int. Conf. Microw. Intell. Mobility*, 2015, pp. 1–4.

[7] C. Waldschmidt, J. Hasch, and W. Menzel, "Automotive radar – from first efforts to future systems," *IEEE J. Microwaves*, vol. 1, no. 1, pp. 135–148, Jan. 2021.

[8] L. Maurer, G. Haider, and H. Knapp, "77 GHz SiGe based bipolar transceivers for automotive radar applications - An industrial perspective," in *Proc. IEEE 9th Int. New Circuits Syst. Conf.*, 2011, pp. 257–260.

[9] J.-S. Kim *et al.*, "79 GHz active array FMCW radar system on low-cost FR-4 substrates," *IEEE Access*, vol. 8, pp. 213 854–213 865, Nov. 2020.

[10] H. Cetinkaya, S. Kueppers, R. Herschel, and N. Pohl, "Millimeter-wave MIMO array based on semi-circular topology," *IEEE Sensors J.*, vol. 20, no. 14, pp. 7740–7749, Jul. 2020.

[11] Texas Instruments Incorporated, "SWRU553 A: AWRx cascaded radar RF evaluation module (MMWCAS-RF-EVM)," Feb. 2020. Accessed: Aug. 13, 2021. [Online]. Available: https://www.ti.com/lit/ug/swru553a/swru553a.pdf

[12] A. Och, C. Pfeffer, J. Schrattenecker, S. Schuster, and R. Weigel, "A scalable 77 GHz massive MIMO FMCW radar by cascading fully-integrated transceivers," in *Proc. Asia-Pacific Microw. Conf.*, 2018, pp. 1235–1237.

[13] M. Kucharski, A. Ergintav, W. A. Ahmad, M. Krstić, H. J. Ng, and D. Kissinger, "A scalable 79-GHz radar platform based on single-channel transceivers," *IEEE Trans. Microw. Theory Techn.*, vol. 67, no. 9, pp. 3882–3896, Sep. 2019.

[14] H. J. Ng, R. Hasan, and D. Kissinger, "A scalable four-channel frequency-division multiplexing MIMO radar utilizing single-sideband delta-sigma modulation," *IEEE Trans. Microw. Theory Techn.*, vol. 67, no. 11, pp. 4578–4590, Nov. 2019.

[15] C. Wagner, H.-P. Forstner, G. Haider, A. Stelzer, and H. Jäger, "A 79-GHz radar transceiver with switchable TX and LO feedthrough in a silicon-germanium technology," in *Proc. IEEE Bipolar/BiCMOS Circuits Technol. Meeting*, 2008, pp. 105–108.

[16] A. Mushtaq, W. Winkler, and D. Kissinger, "A 79-GHz scalable FMCW MIMO automotive radar transceiver architecture with injection-locked synchronization," in *Proc. IEEE MTT-S Int. Microw. Symp.*, 2019, pp. 690–693.

[17] A. Dürr, D. Schwarz, and C. Waldschmidt, "A system analysis of noise influences on the imaging performance of millimeter wave MIMO radars," in *Proc. IEEE/MTT-S Int. Microw. Symp.*, 2020, pp. 1019–1022.

[18] A. Dürr *et al.*, "High-resolution 160-GHz imaging MIMO radar using MMICs with on-chip frequency synthesizers," *IEEE Trans. Microw. Theory Techn.*, vol. 67, no. 9, pp. 3897–3907, Sep. 2019.

[19] R. Adler, "A study of locking phenomena in oscillators," *Proc. IRE*, vol. 34, no. 6, pp. 351–357, Jun. 1946.

[20] T. Djurhuus and V. Krozer, "Theory of injection-locked oscillator phase noise," *IEEE Trans. Circuits Syst. I, Reg. Papers*, vol. 58, no. 2, pp. 312–325, Feb. 2011.

[21] E. Shumakher and G. Eisenstein, "On the noise properties of injection-locked oscillators," *IEEE Trans. Microw. Theory Techn.*, vol. 52, no. 5, pp. 1523–1537, May 2004.
[22] B. Razavi, "A study of injection locking and pulling in oscillators," *IEEE J. Solid-State Circuits*, vol. 39, no. 9, pp. 1415–1424, Sep. 2004.
[23] A. Dürr, R. Kramer, D. Schwarz, M. Geiger, and C. Waldschmidt, "Calibration-based phase coherence of incoherent and quasi-coherent 160-GHz MIMO radars," *IEEE Trans. Microw. Theory Techn.*, vol. 68, no. 7, pp. 2768–2778, Jul. 2020.
[24] M. C. Budge and M. P. Burt, "Range correlation effects in radars," in *Proc. IEEE Nat. Radar Conf.*, 1993, pp. 212–216.
[25] V. Winkler, "Range doppler detection for automotive FMCW radars," in *Proc. Eur. Radar Conf.*, 2007, pp. 166–169.
[26] A. Dürr, B. Schneele, D. Schwarz, and C. Waldschmidt, "Range-angle coupling and near-field effects of very large arrays in mm-wave imaging radars," *IEEE Trans. Microw. Theory Techn.*, vol. 69, no. 1, pp. 262–270, Jan. 2021.
[27] D. Pozar, *Microwave Engineering*, 4th ed. Hoboken, NJ, USA: Wiley, 2012.
[28] K. Thurn, R. Ebelt, and M. Vossiek, "Noise in homodyne FMCW radar systems and its effects on ranging precision," in *IEEE MTT-S Int. Microw. Symp. Dig.*, 2013, pp. 1–3.
[29] S. Scherr, S. Ayhan, B. Fischbach, A. Bhutani, M. Pauli, and T. Zwick, "An efficient frequency and phase estimation algorithm with CRB performance for FMCW radar applications," *IEEE Trans. Instrum. Meas.*, vol. 64, no. 7, pp. 1868–1875, Jul. 2015.
[30] C. Candan, "A method for fine resolution frequency estimation from three DFT samples," *IEEE Signal Process. Lett.*, vol. 18, no. 6, pp. 351–354, Jun. 2011.
[31] S. Scherr *et al.*, "Influence of radar targets on the accuracy of FMCW radar distance measurements," *IEEE Trans. Microw. Theory Techn.*, vol. 65, no. 10, pp. 3640–3647, Oct. 2017.

DOMINIK SCHWARZ (Graduate Student Member, IEEE) received the M.Sc. degree from Ulm University, Ulm, Germany, in 2018, where he is currently working toward the Ph.D. degree.

From 2011 to 2018, he was a Student Trainee with Hensoldt Sensors, Ulm, Germany. In 2018, he joined the Institute of Microwave Engineering, Ulm University. His current research interests include automotive MIMO radars with a focus on high bandwidths, high channel counts, 2D-DoA estimation, and novel multilayer PCB structures at millimeter-wave frequencies.

Mr. Schwarz was a recipient of the Ingenieure für Kommunikation (IfKom) Award in 2016 and the Argus Science Award in 2019.

CHRISTIAN MEYER received the M.Sc. degree from Ulm University, Ulm, Germany, in 2020.

From 2016 to 2018, he was an Intern with TELEFUNKEN Radio Communication Systems GmbH & Co. KG, Ulm, Germany. In 2020, he joined Diehl Defence GmbH & Co. KG, Röthenbach an der Pegnitz, Germany.

ANDRÉ DÜRR (Graduate Student Member, IEEE) received the M.Sc. degree from Ulm University, Ulm, Germany, in 2017, where he is currently working toward the Ph.D. degree.

From 2015 to 2016, he was an Intern with Bosch Research and Technology Center North America, Palo Alto, CA, USA. In 2017, he joined the Institute of Microwave Engineering, Ulm University. His current research interests include novel imaging radar sensor concepts, phase noise mitigation, and performance degradation of noncoherent multichannel radar systems and their synchronization, all at millimeter-wave frequencies.

Mr. Dürr was a recipient of the Argus Science Award in 2015, the Verband der Elektrotechnik Elektronik Informationstechnik (VDE) Award in 2015, and the Verband Deutscher Ingenieure (VDI) Award in 2017.

AHMAD MUSHTAQ (Member, IEEE) received the M.Sc. degree with specialization in communication electronics from Technical University of Munich, Munich, Germany, in 2016.

Since 2016, he is an RFIC Designer with Silicon Radar GmbH, Frankfurt (Oder). His research interests include mm-wave radar circuit design, optimization, and radar system behavioral modeling for various industrial and consumer applications.

WOLFGANG WINKLER (Member, IEEE) received the Dipl.-Ing. (M.S.E.E.) and Dr.-Ing. (Ph.D.E.E.) degrees from Technical University Ilmenau, Ilmenau, Germany, in 1979 and 1984, respectively.

From 1979 to 1984, he was a Research Assistant with the Institute for Physics and Technology of Electron Devices, Technical University Ilmenau, working in the field of research and development of CCD and dynamic RAM devices. Since 1984, he has been a Design Engineer with Semiconductor Research Institute IHP in Frankfurt (Oder) where he was involved in development of CMOS and BiCMOS technologies and starting in 1998 he worked in the field of high frequency circuit design at IHP. His main research interests included benchmarking circuits for technology characterization and model verification and circuits for wireless communication and radar in silicon-based technologies. Main projects were building blocks for wireless transceivers at 60 GHz and radar circuits for automotive radar frequencies at 24 GHz and 77 GHz. In 2006, he founded the company Silicon Radar GmbH, Frankfurt (Oder), Germany, and was CTO for many years and is now innovation Manager in this company. At Silicon Radar, he headed the design of integrated circuits for plenty of radar-applications for example for low-cost automotive radar, for industrial use and for consumer products. Main technology of the circuits was state-of-the-art Silicon-Germanium BiCMOS. He brought several innovative integrated circuit types to series production. Among others it is the first highly-integrated 122 GHz ISM-band radar transceiver that is in volume production since 2017.

CHRISTIAN WALDSCHMIDT (Senior Member, IEEE) received the Dipl.-Ing. (M.S.E.E.) and Dr.-Ing. (Ph.D.E.E.) degrees from the University Karlsruhe (TH), Karlsruhe, Germany, in 2001 and 2004, respectively.

From 2001 to 2004, he was a Research Assistant with the Institut für Höchstfrequenztechnik and Elektronik (IHE), Universität Karlsruhe (TH), Germany. Since 2004, he has been with Robert Bosch GmbH in the business units Corporate Research and Chassis Systems. He was heading different research and development teams in microwave engineering, RF-sensing, and automotive radar. In 2013, he returned to academia and was appointed as the Director of the Institute of Microwave Engineering, University Ulm, Germany, as a Full Professor. He authored or coauthored more than 200 scientific publications and more than 20 patents. His research interests include radar and RF-sensing, mm-wave and submillimeter-wave engineering, antennas and antenna arrays, and RF and array signal processing.

Prof. Waldschmidt is a member of the Executive Committee Board of the German MTT/AP Joint Chapter and a member of the German Information Technology Society (ITG). He was the Chair of the IEEE MTT-27 Technical Committee on wireless enabled automotive and vehicular applications. He was a two-time TPC Chair and the General Chair of the IEEE MTT International Conference on Microwaves for Intelligent Mobility. Since 2018, he has been an Associate Editor for IEEE MICROWAVE AND WIRELESS COMPONENTS LETTERS. He is a reviewer for multiple IEEE transactions and many IEEE conferences in the field of microwaves. He was a co-recipient of 11 best paper awards since 2014.